Available online at www.sciencedirect.com
SCIENCE DIRECT
Journal of Organometallic Chemistry 691 (2006) 3213–3222
Journal of Organometallic Chemistry
www.elsevier.com/locate/jorganchem

Synthesis and structure of functional spherosilicate building block molecules for materials synthesis

Jason C. Clark [a], Suree Saengkerdsub [b], Geoff T. Eldridge [a], C. Campana [c], Craig E. Barnes [a,*]

[a] Department of Chemistry, University of Tennessee – Knoxville, Knoxville, TN 37996-1600, USA
[b] Chemical Sciences Division, Oak Ridge National Laboratory, Oak Ridge, TN 37831, USA
[c] Bruker AXS Inc., Madison Wisconsin, WI 53711-5373, USA

Received 31 August 2005; received in revised form 14 March 2006; accepted 14 March 2006
Available online 21 March 2006

Abstract

Cubic, trialkyl tin functionalized spherosilicates $Si_8O_{20}(SnR_3)_8$ (R = Me, ^{n}Bu) and the pentagonal prismatic tin-spherosilicate $Si_{10}O_{25}(SnMe_3)_{10}$ have been synthesized and characterized. Single crystal X-ray structures were obtained for $Si_8O_{20}(SnMe_3)_8$ (**I**), $Si_8O_{20}(SnMe_3)_8 \cdot 4H_2O$ (**I · 4H$_2$O**), and $Si_{10}O_{25}(SnMe_3)_{10} \cdot 4H_2O$ (**II**). Structural metrics for the silicate cores observed in these structures were compared to other Si_8O_{12} and $Si_{10}O_{25}$ cores reported in the CSD database. A pronounced tetragonal distortion of the Si_8O_{20} cage leads to Si–O–Si bond angles that are considerably distorted in **I · 4H$_2$O** when compared to other analogous Si_8O_{12} structures described in the literature. These octameric stannylated spherosilicates readily react with metal chlorides to produce mesocopically interesting metal oxide and hybrid materials. An illustration of this is found in the reaction of the octameric anhydrous tin compound **I** with titanocene dichloride to give the octatitanocene derivative $Si_8O_{20}(Cp_2TiCl)_8 \cdot 3CH_2Cl_2$ (**III**). The single crystal structure of **III** is also described.

Keywords: Silicate cage precursor; Silicate decamer; Silicate octomer; Zeolite building block; Spherosilicates; Structural distortions spherosilicates; Silicate oxide; Titanocene dichloride; Trimethyl tin; Aprotic building block synthesis

1. Introduction

Spherosilicates are molecular cage compounds of the general formula $(XSiO_{1.5})_n$ (X = inorganic or organic substituents, $n = 6$, 8, 10, 12, 14) comprised of Si–O–Si based rings which result from oxygen shared $XSiO_3$ tetrahedral units [1]. These compounds are interesting from both application and fundamental perspectives. They are useful in a broad range of areas including atomic scavengers, cores for branched dendritic macromolecules, molecular composite materials, optical fibers and cosmetics [2–6]. They are structurally important because the cubic Si_8O_{12} and the pentagonal prismatic $Si_{10}O_{15}$ cages contain double four ring (D4R) and double five ring (D5R) units, respectively. Both D4R and D5R ring units are also found in many natural and synthetic zeolites and silicates [7,8]. Due to the occurrence of such units in these interesting materials, spherosilicate based compounds have been used as models in several structural and vibrational model studies [7–11].

Materials scientists have also employed spherosilicates as building blocks in developing new materials [1]. Several schemes have been developed to attach synthetically useful groups to the *exo*cage positions [1,12–16]. Once functionalized, these silicate building blocks can be used as polyfunctional monomers that may be cross-linked together to produce three-dimensional silicate polymers. For example, high surface area materials have been made from the sol–gel polymerization of $(CH_3O)_8Si_8O_{12}$ while multicomponent, porous inorganic materials were synthesized by reacting $Si_8O_{20}[N(CH_3)_3(C_2H_4OH)]_8 \cdot nH_2O$ with

* Corresponding author.
E-mail address: cebarnes@utk.edu (C.E. Barnes).

0022-328X/$ - see front matter © 2006 Elsevier B.V. All rights reserved.
doi:10.1016/j.jorganchem.2006.03.028

$Zr(C_5H_7O_2)_4$ [17–19]. Inorganic/organic hybrid porous materials have been made by linking Si_8O_{12} units together with organic groups of various lengths via a hydrosilylation reactions [20,21]. These cross-linked hybrid materials have also been studied theoretically [22].

Cubic spherosilicates bearing *exo*cage trialkyltin functional groups are reactive towards many metal halides via a metathesis reaction whereby novel metallosilicate materials are produced [14,23,24]. It has recently been shown that the nanometer size associated with Si_8O_{12} units allows for tailoring of the immediate chemical environment in such metallosilicates [23]. Herein we describe the synthesis and structures of several cubic and pentagonal prismatic stannylated spherosilicates $Si_8O_{20}(SnR_3)_8$ (R = Me and ^{n}Bu) and $Si_{10}O_{25}(SnMe_3)_{10}$. Furthermore, $Si_8O_{20}(SnMe_3)_8$ has been used to synthesize the octatitanocene derivative, $Si_8O_{20}(Cp_2TiCl)_8$. Structural comparisons of these compounds with related spherosilicates reveal new insights into their properties as potential building blocks in the preparation of nanostructured silicate materials.

2. Experimental

Solution nuclear magnetic resonance (NMR) spectra were recorded at 9.4 T on a broadband Bruker Avance (400 MHz ^{1}H) spectrometer. Chemical shifts were referenced to the following: ^{1}H NMR δ (C_6D_5H) 7.15 ppm; ^{13}C NMR δ (C_6D_6) 128.39 ppm; ^{119}Sn δ (Me_4Sn) 0 ppm; and ^{29}Si δ (Me_4Si) 0 ppm.

Single crystal structures were determined using a Bruker AXS Smart 1000 X-ray diffractometer equipped with a CCD area detector with a graphite monochromated Mo source (Kα radiation, $\lambda = 0.71073$ Å). The instrument was fitted with an upgraded model LT-2 low-temperature controller. Crystals coated with paratone oil (Exxon) were mounted on a "hair loop" under a nitrogen stream at −100 °C. Global refinement of unit cell and orientation matrix data and data reductions were performed using SAINT 6.02 [25]. All calculations were performed using the SHELXTL 5.1 proprietary software package [25]. The SADABS program was used to make empirical adsorption corrections [26]. Listings of atom coordinates, bond distances, angles, atomic displacement factors, and H-atom coordinates may be found in Supplementary information to the manuscript.

Elemental analyses were performed by Desert Analytics (Tucson, AZ) unless otherwise noted. Thermal gravimetric analysis (TGA) was performed on a TA Instruments Q50 TGA equipped with platinum pans. Nitrogen was used as the purge gas for both the balance and in the furnace. Infrared experiments were performed on a Biorad FTS-60A FTIR spectrometer.

Structural parameters from single crystal X-ray data for compounds containing the cubic Si_8O_{12} and pentagonal prismatic $Si_{10}O_{15}$ spherosilicate fragments were obtained from the Cambridge Structural Database (CSD) [27]. Seventy structures containing the Si_8O_{12} cubic spherosilicate fragment were found in the CSD database. Structural information was available for 36 compounds, 18 of which were molecules containing the Si_8O_{20} core [2,15,28–58]. Four compounds containing the $Si_{10}O_{15}$ core were found in the CSD database [2,51,59].

2.1. Synthesis of $Si_8O_{20}(SnMe_3)_8 \cdot 4H_2O$

Compound **I · 4H$_2$O** was synthesized according to the procedures of Feher and Waller with minor modifications [14]. Octahydridosilsesquioxane, $H_8Si_8O_{12}$ was added portion wise to a solution of bis(trimethyltin)oxide, $(Me_3Sn)_2O$ in toluene under nitrogen [14,60,61]. The reaction was monitored via ^{1}H NMR. After stirring overnight, removal of the volatiles resulted in a white powder which was recrystallized from hexanes in air to give white, needle shaped crystals upon cooling to 5 °C overnight (6.77 g, 3.65 mmol, 91% based on $H_8Si_8O_{12}$). X-ray quality crystals of the tetrahydrate were obtained from benzene solution via evaporation. ^{1}H NMR δ 0.36 (s) $^2J(^{117}SnH, ^{119}SnH) =$ 56.1, 59.4 Hz, $^1J(CH) = 130.9$ Hz; ^{13}C: δ −2.92 (s) $^1J(^{117}SnC, ^{119}SnC) = 387.5$, 405.4 Hz; ^{119}Sn: δ 118.67 (s); and ^{29}Si: δ −101.144 (s) $^2J(SiSn) = 12.4$ Hz.

The overall molecular structure was verified by its single crystal X-ray structure. Four H_2O molecules per $Si_8O_{20}(SnMe_3)_8$ were found in the crystal. TGA analysis of the crystals showed approximately a 4% weight loss at 100 °C in air, consistent with the loss of four water molecules (3.74% theoretical weight loss). TGA also shows that the compound melts at 180 °C and begins to decompose in air around 250 °C.

Compound **I · 4H$_2$O** was heated to 100 °C under vacuum overnight and recrystallized from dry hexanes at 5 °C under nitrogen to produce anhydrous **I** suitable for X-ray analysis.

2.2. Synthesis of $Si_8O_{20}(Sn^nBu_3)_8$

Bis(tri-*n*-butyltin)oxide, $O(SnBu^n_3)_2$ (Gelest, Inc.) was distilled and degassed prior to use. 2.00 g (4.71 mmol) of $H_8Si_8O_{12}$, was added to a magnetically stirred round-bottomed flask containing a 5% stoichiometric excess of the tin ether, $O(SnBu^n_3)_2$ at 0 °C under a nitrogen atmosphere. The reaction was allowed to proceed for one hour. After warming to room temperature, the reaction flask was fitted with a short path distillation head. Both tri-*n*-butyltinhydride and excess $O(SnBu^n_3)_2$ were removed via vacuum distillation.

The resulting product, $Si_8O_{20}(SnBu^n_3)_2$, is a sticky, white solid. Recovered yields are 95–98%. No clear melting point could be observed upon heating. ^{1}H NMR: δ 1.09 (t, 72H), δ 1.38 (t, 48H) δ 1.54 (m, 48H), δ 1.84 (m, 48H); ^{13}C: δ 14.2 (s), δ 16.4 (s) $^1J(SnC) = 356$, 373 Hz, δ 27.7 (s) $^3J(SnC) =$ 60.3, 63.1 Hz, δ 28.4 (s) $^2J(SnC) = 17.8$ Hz; ^{119}Sn: (149.18 MHz, C_6D_6) δ 85.9 (s); and ^{29}Si: δ −101.0 (s). Elemental analysis: found 40.40% C and 7.57% H, calculated for $Si_8Sn_8O_{20}C_{96}H_{216}$: 40.24% C and 7.60% H.

2.3. Synthesis of $Si_{10}O_{25}(SnMe_3)_{10} \cdot 4H_2O$ (II)

The procedure for the preparation of $Si_{10}O_{25}(SnMe_3)_{10}$ is similar to that of $Si_8O_{20}(SnMe_3)_8$. To a solution of $(Me_3Sn)_2O$ in toluene, a mixture of (1:1) $H_8Si_8O_{12}$ and $H_{10}Si_{10}O_{15}$ was added stepwise until all $(Me_3Sn)_2O$ had reacted as indicated by ^1H NMR [60]. The resulting mixture of $Si_{10}O_{25}(SnMe_3)_{10}$ and $Si_8O_{12}(SnMe_3)_8$ was separated by fractional crystallization from hexanes. The first crop of crystals grown at 5 °C was found to be pure $Si_8O_{12}(SnMe_3)_8$ according to ^1H NMR and the second crop was 93% $Si_{10}O_{25}(SnMe_3)_{10}$ and 3% $Si_8O_{20}(SnMe_3)_8$. The crystalline product was analyzed using multinuclear NMR as follows: ^1H NMR δ 0.42 (s) $^2J(^{117}SnH, ^{119}SnH) = 56.7, 59.4$ Hz, $^1J(CH) = 130.3$ Hz; ^{13}C: δ −2.80 (s) $^1J(^{117}SnC, ^{119}SnC) = 386.8, 404.6$ Hz; ^{119}Sn: δ 116.21 (s); and ^{29}Si: δ −101.9 (s) $^2J(SiSn) = 12.5$ Hz.

The overall molecular structure of the tetrahydrate $Si_{10}O_{25}(SnMe_3)_{10} \cdot 4H_2O$ was verified by single crystal X-ray analysis. Four H_2O molecules per $Si_{10}O_{25}(SnMe_3)_{10}$ were found in the crystal before heating under vacuum. TGA analysis of the crystals showed approximately a 3% weight change between 35 and 90 °C. This is consistent with the loss of four water molecules (3.01% theoretical weight loss). The compound melts at 166 °C and begins to decompose in air around 250 °C (TGA). Elemental analysis: found 15.08% C and 4.26% H, calculated for $Si_{10}Sn_{10}O_{25}C_{30}H_{90} \cdot 4H_2O$: 15.07% C and 4.13% H.

2.4. Synthesis of $Si_8O_{20}(Cp_2TiCl)_8 \cdot 3CH_2Cl_2$ (III)

$Si_8O_{20}(SnMe_3)_8$ (0.47 g, 0.25 mmol, 2.0 mmol $SnMe_3$ reaction site) was weighed into one side of a double well Schlenk vessel separated by a frit while Cp_2TiCl_2 (1.04 g, 4.1 mmol, 2.1 eq/$SnMe_3$) was weighed into the other side. Methylene chloride was vapor transferred under vacuum onto both reactants. The reaction was started when the $Si_8O_{20}(SnMe_3)_8$ solution was poured through the medium frit and mixed with the Cp_2TiCl_2 solution. At 50 °C, yellow microcrystals gradually precipitated out from the deep red solution. The reaction was stopped by removing all volatiles after 2.5 h. The golden yellow microcrystalline $Si_8O_{20}(Cp_2TiCl)_8$ was washed with methylene chloride several times until the orange-red color of Cp_2TiCl_2 was not observed in the wash solution. After the removal of methylene chloride, pure $Si_8O_{20}(Cp_2TiCl)_8$ was obtained (0.470 g, 0.21 mmol, 84% yield).

The multinuclear NMR was as follows: ^1H NMR δ 6.24 (s); ^{13}C NMR δ −118.50 (s); ^{29}Si NMR δ −106.34 (s). The overall molecular structure was verified by single crystal X-ray analysis. Three CH_2Cl_2 solvate molecules per $Si_8O_{20}(Cp_2TiCl)_8$ were found in the crystal. Elemental analysis (Robertson Microlit Laboratories, Inc.): found: 44.2% C and 4.30% H, calculated for $Si_8O_{20}Ti_8Cl_8C_{80}H_{80}$: 44.09% C and 4.04% H.

3. Results and discussion

The general approach to the synthesis of trialkyl tin substituted spherosilicates was first described by Feher and Weller [14]. Reaction of tin ethers $R_3Sn–O–SnR_3$ with Si–H functionalities to produce mixed silicon–tin ethers (≡Si–O–Sn≡) proceeds smoothly and in high yield. In the case of the decatin cage complex, $Si_{10}O_{25}(SnMe_3)_{10}$, the silicon hydride precursor can only be isolated as a mixture with the octamer, $Si_8O_{12}H_8$. Titration of the mixture with the trimethyl tin ether gave the corresponding tin products cleanly. Fractional crystallization gave pure samples of the decatin compound **II**, for characterization.

The tin-substituted spherosilicates react with many high valent transition metal and main group chlorides (e.g. $AlCl_3$, $SiCl_4$, $TiCl_4$, $VOCl_3$) to cleanly metathesize the trialkyl tin group for the metal chloride (Eq. (1)) [23,24]. The reaction of titanocene dichloride Cp_2TiCl_2, with **I** illustrates the utility of this reaction. At room temperature, Cp_2TiCl_2 reacts with $Si_8O_{20}(SnMe_3)_8$ in a variety of organic solvents to produce the titanocene substituted spherosilicate, $Si_8O_{12}(OCp_2TiCl)_8$ (**III**).

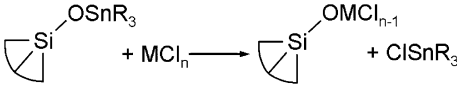

(1)

Under the conditions used, only one of the two chloride ligands on titanocene dichloride reacts. In this case and for other polychlorides, adjusting of the conditions of the reaction and stoichiometric ratios of reactants leads to a general methodology for the designed preparation of tailored mixed metal–silicate building block materials [23,24]. Complete structural, elemental and spectroscopic characterization data for compounds **I–III** are given in Section 2 and following discussion.

3.1. Structural characterization of $Si_8O_{20}(SnMe_3)_8 \cdot 4H_2O$ ($\mathbf{I \cdot 4H_2O}$)

$Si_8O_{20}(SnMe_3)_8 \cdot 4H_2O$ crystallizes in the $P\bar{1}$ space group. Structure and refinement data are given in Table 1. The structure of the octakis trimethyltin silicate tetrahydrate ($\mathbf{I \cdot 4H_2O}$) in the crystal may be described as a distorted, cubic Si_8O_{12} cage surrounded by eight trimethyl tin groups bound to the eight oxygen atoms external to the silicate cage (Fig. 1). Only one half of the molecule is unique by virtue of crystallographically imposed inversion symmetry at the center of the Si_8O_{12} cage. The crystal also contains four water molecules (two unique) present as Lewis base adducts coordinated to tin in two of the unique trimethyltin groups.

The Si_8O_{12} core exhibits a significant tetragonal distortion from ideal cubic symmetry by having two opposite Si_4O_4 faces of the cube pulled away from each other. The four Si–O–Si cage edges parallel to the distortion axis accommodate this elongation by opening up the Si–O–Si angles around oxygen until they are close to linear (average

Table 1
Crystal data and structure refinement for compounds **I**–**III**

Identification code	**I**	**I · 4H$_2$O**	**II**	**III**
Molecular formula	$Si_8O_{20}(SnMe_3)_8$	$Si_8O_{20}(SnMe_3)_8 \cdot 4H_2O$	$Si_{10}O_{25}(SnMe_3)_{10} \cdot 4H_2O$	$Si_8O_{20}(TiClCp_2)_8 \cdot 2CH_3Cl$
Formula weight	1855.06	1927.12	2390.88	2507.74
Temperature (K)	173(2)	293(2)	173(2)	198(2)
Wavelength (Å)	0.71073	0.71073	0.71073	0.71073
Crystal system	Triclinic	Triclinic	Orthorhombic	Triclinic
Space group	$P\bar{1}$	$P\bar{1}$	*Pbca*	$P\bar{1}$
a (Å)	11.339(3)	11.2046(6)	21.834(5)	13.6919(5)
b (Å)	11.569(3)	12.0644(6)	26.567(7)	14.1160(5)
c (Å)	13.258(3)	12.3545(6)	28.037(7)	14.2380(5)
α (°)	68.973(4)	86.6650(10)	90	101.9820(10)
β (°)	76.426(4)	81.8930(10)	90	99.8590(10)
γ (°)	71.264(4)	85.4890(10)	90	107.7540(10)
Volume (Å^3)	1523.2(7)	1646.35(14)	1626.4(7)	2481.12(15)
Z	1	1	8	1
D_{calc} (Mg/m^3)	2.022	1.944	1.953	1.678
Absorption coefficient (mm^{-1})	3.436	3.187	3.224	1.149
F(000)	888	928	9200	1270
Crystal size (mm^3)	0.5 × .05 × 0.5	0.5 × 0.4 × 0.4	0.20 × 0.15 × 0.10	0.2 × 0.2 × 0.05
θ Range for data collection (°)	1.91–23.32	1.67–28.28	1.41–23.27	1.51–27.65
Index ranges	$-12 \leqslant h \leqslant 12$, $-12 \leqslant k \leqslant 12$, $-14 \leqslant l \leqslant 14$	$-14 \leqslant h \leqslant 14$, $-15 \leqslant k \leqslant 16$, $-15 \leqslant l \leqslant 16$	$-23 \leqslant h \leqslant 24$, $-29 \leqslant k \leqslant 29$, $1-31 \leqslant l \leqslant 31$	$-17 \leqslant h \leqslant 17$, $-18 \leqslant k \leqslant 18$, $-18 \leqslant l \leqslant 18$
Reflections collected	11 644	17 832	120 540	27 306
Independent reflections (R_{int})	4387 (0.0182)	7705 (0.0240)	11 673 (0.0641)	27 306
Completeness to *θ*	23.32°: 99.4%	28.28°: 94.4%	23.27°: 99.7%	27.65°: 96.4%
Absorption correction	Semi-empirical from equivalents	Semi-empirical from equivalents	Semi-empirical from equivalents	Semi-empirical from equivalents
Refinement method	Full-matrix least-squares on F^2	Full-matrix least-squares on F^2	Full-matrix least-squares on F^2	Full-matrix least-squares on F^2
Data/restraints/parameters	4387/0/283	7705/5/317	11 673/16/806	27 306/3718/1022
Goodness-of-fit on F^2	1.026	1.135	1.216	1.021
Final *R* indices [$I > 2\sigma(I)$]	$R_1 = 0.0261$, $wR_2 = 0.00733$	$R_1 = 0.0243$, $wR_2 = 0.0634$	$R_1 = 0.0323$, $wR_2 = 0.0790$	$R_1 = 0.0670$, $wR_2 = 0.1694$
R indices (all data)	$R_1 = 0.0292$, $wR_2 = 0.0760$	$R_1 = 0.0267$, $wR_2 = 0.0647$	$R_1 = 0.0637$, $wR_2 = 0.1137$	$R_1 = 0.0884$, $wR_2 = 0.1860$
Largest difference in peak and hole (e Å^{-3})	2.059 and −0.411	0.363 and −1.802	2.547 and −0.888	0.876 and −0.948

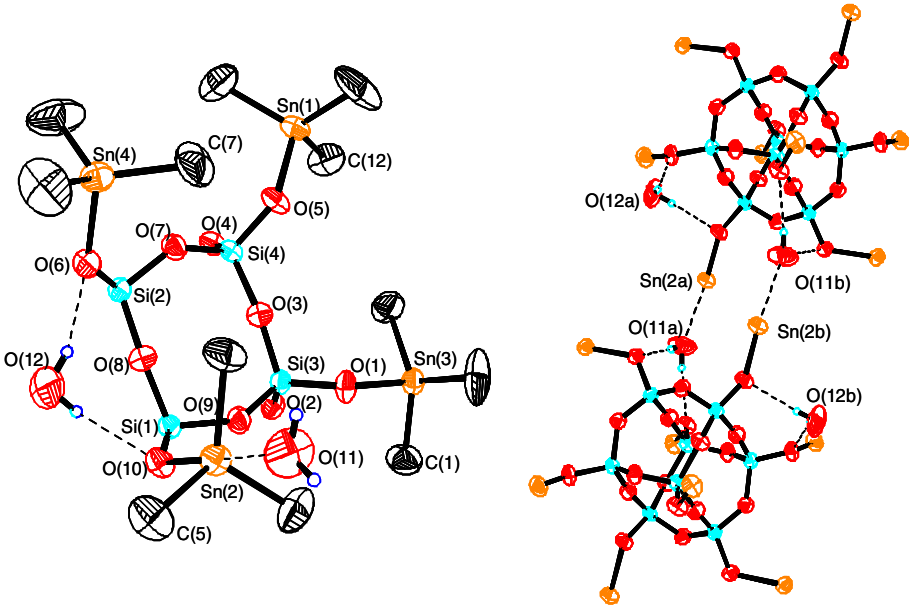

Fig. 1. Single crystal X-ray structure of $Si_8O_{20}(SnMe_3)_8 \cdot 4H_2O$. The crstallographically unique part of the molecule is shown along with interaction between two $Si_8O_{20}(SnMe_3)_8$ and two H_2O molecules.

angle 172°). The Si–O bond lengths along these edges and along other Si_4O_4 edges of the cube are not lengthened appreciably over average bond distances observed in similar silicate cage structures (vide infra).

The oxygen atoms of the two water molecules in the crystal are within bonding distance (Sn(3)–O(12) 2.645 Å; Sn(2)–O(11) 2.799 Å) to two tin atoms of trimethyl tin groups in the crystal and positioned *trans* to the terminal oxygens of the cage (Fig. 1) [62–71]. The three methyl groups are almost coplanar with the tin atom in each case producing a trigonal bipyramidal coordination geometry around tin. The other two unique trimethyl tin groups in the structure have overall tetrahedral arrangements of the three methyl groups and one terminal oxygen atom bound to tin.

The hydrogen atoms of the water molecules in the crystal are directed away from the trimethyltin group to which the oxygen is interacting and form hydrogen bonds to two *exo*cage oxygen atoms of a neighboring silicate cube in the lattice (Fig. 1). It is interesting to note that in both cases two hydrogen bonds from one water molecule (O(12)) bracket an elongated edge (Si(1)–O(8)–Si(2)) of the Si_8O_{12} core.

The combination of $Sn\cdots O_{water}$ Lewis base interactions and hydrogen bonding described above produces a two-dimensional ordering of $Si_8O_{20}(SnMe_3)_8$ molecules in the solid state. Planes of $Si_8O_{20}(SnMe_3)_8$ molecules in the crystal, linked through water can clearly be seen in molecular packing diagrams (Fig. 2). No unusual or strong intermolecular contacts are observed between planes in the lattice.

3.2. Structural characterization of anhydrous $Si_8O_{20}(SnMe_3)_8$ (**I**)

$Si_8O_{20}(SnMe_3)_8$ crystallizes in the $P\bar{1}$ space group. Structure and refinement data are given in Table 1. While the overall structure of anhydrous $Si_8O_{20}(SnMe_3)_8$ (**I**) in the solid state is similar to that of the tetrahydrate, significant differences exist (Fig. 3). In contrast to the tetrahydrate structure, the substituent geometry around all tin atoms is tetrahedral. Also, the distortion of the cubic silicate cage is not nearly as pronounced. The largest Si–O–Si cage angles in this structure are 159.8(2)° and 161.2(2)° which is ~11° less than what is observed in the structure of the hydrate. No ordering of $Si_8O_{20}(SnMe_3)_8$ molecules into sheets is observed in the crystal of anhydrous **I**.

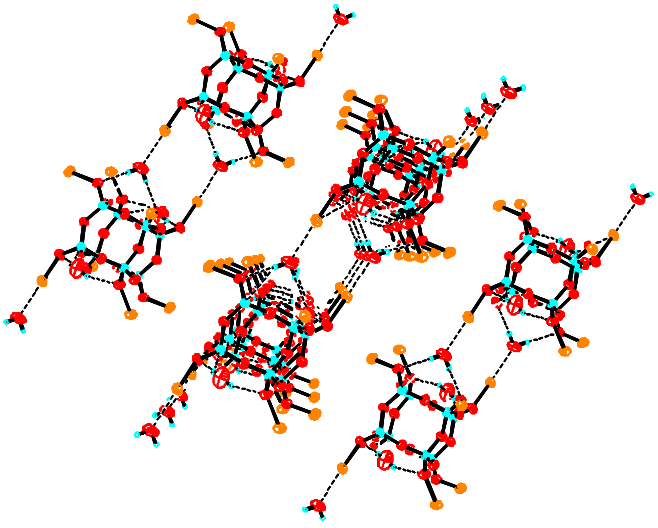

Fig. 2. Packing diagram of $Si_8O_{20}(SnMe_3)_8\cdot 4H_2O$. Hydrogen bonding and Lewis base interactions of the two water molecules with the $Si_8O_{20}(SnMe_3)_8$ molecules results in two-dimensional sheets.

3.3. Structural characterization of $Si_8O_{20}(Cp_2TiCl)_8\cdot 3CH_2Cl_2$ (**III**)

Data were collected on a nonmerohedrally twinned crystal of $Si_8O_{20}(Cp_2TiCl)_8\cdot 3CH_2Cl_2$ having two domains related by a 180° rotation along the $-1\,1\,0$ axis in real space. The reflection file was sorted between the two twin components which are estimated to occur at a 20:80 split in the crystal. Reflections fell into three groups: completely resolved, partially overlapping and completely overlapping. SAINT (version 6.02) successfully derived integrated intensities for all but a few reflections from both twin components in all categories using a single BASF scale factor of 0.21. Both independent data sets from the two twin components were used in the refinement of the model. Structure and refinement data are summarized in Table 1.

The structural model developed for $Si_8O_{20}(Cp_2TiCl)_8\cdot 3CH_2Cl_2$ involves a combination of crystallographically imposed symmetry and disorder. The disorder is found in the titanocene groups and in the methylene chloride solvate molecules. Because of the disorder in the titanocene fragments of the molecule all Cp rings were restrained to be planar and titanium atoms Ti(3) and Ti(4), along with their respective disorder partners (Ti(3′), Ti(4′)) were modeled with equivalent atomic displacement parameters. Fig. 4 shows the structure of $Si_8O_{20}(Cp_2TiCl)_8$ without the disorder in the titanocene groups.

Only half of the central Si_8O_{20} core and its Cp_2TiCl substituents are unique due to the presence of crystallographically imposed inversion symmetry at the center of the cube. There is no disorder in the central Si_8O_{20} core. The disorder in the titanocene groups is illustrated in Fig. 5 and may be described as follows. In two cases, only the Cp rings bound to Ti(1) and Ti(2) are disordered. In both, two sets of overlapping Cp rings were found. Surprisingly, only one refineable chlorine atom position could be identified. The thermal ellipsoid for this chlorine atom is larger than usual which could indicate the presence of two Cl atom positions that are close together and not resolved with the data in hand. Attempts to model this as two distinct atoms were not successful. The occupation of the two components in both cases was modeled by a standard floating occupancy free variable and was found to be approximately 1:1 for the case of Ti(1) and approximately 3:1 for the case of Ti(2).

The other two unique titanocene groups in the molecule (Ti(3) and Ti(4)) exhibit almost identical disorder originating in two distinct positions of the titanium atoms (Fig. 5).

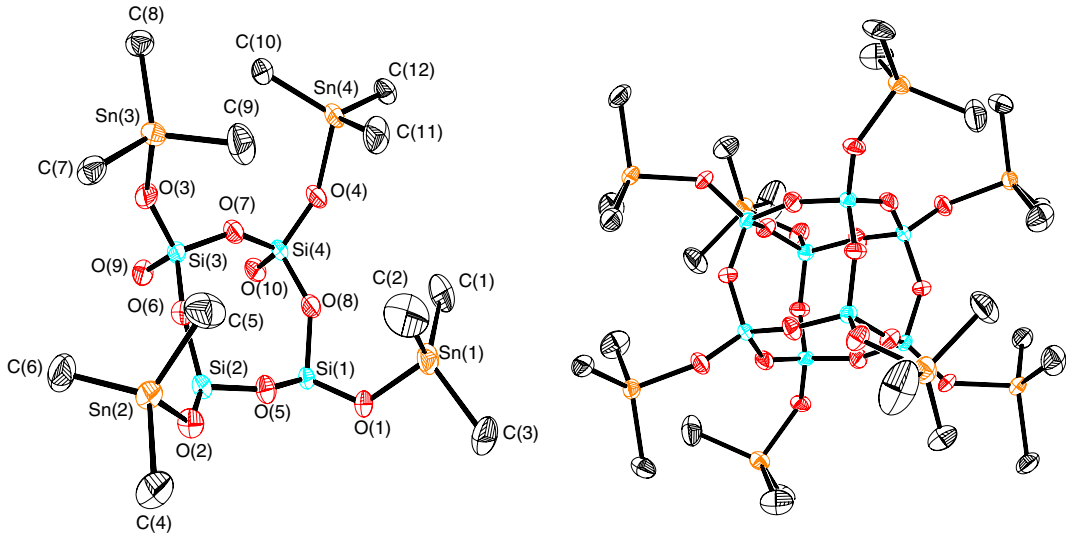

Fig. 3. Single crystal X-ray structure of $Si_8O_{20}(SnMe_3)_8$. The crystallographically unique part is shown along with the entire molecule.

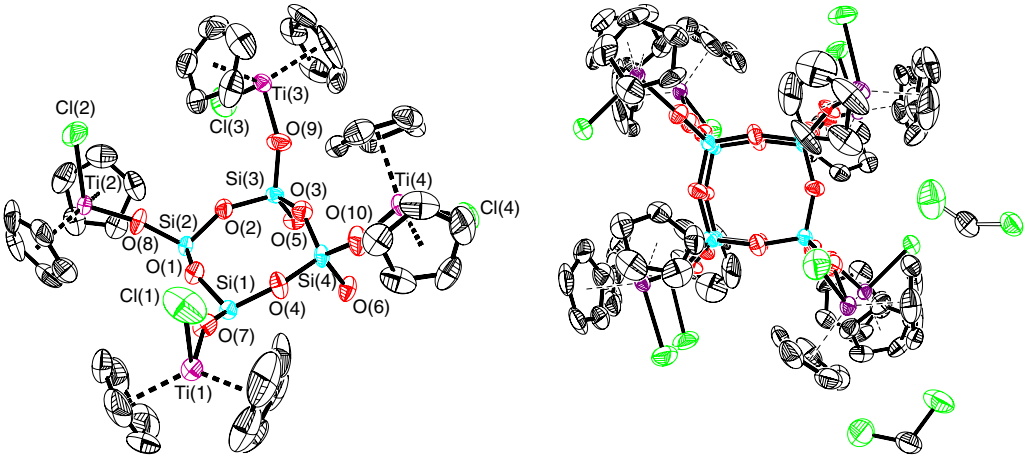

Fig. 4. Single crystal X-ray structure of $Si_8O_{20}(Cp_2TiCl)_8 \cdot 3CH_2Cl_2$. The crystallographically unique part is shown along with the entire molecule.

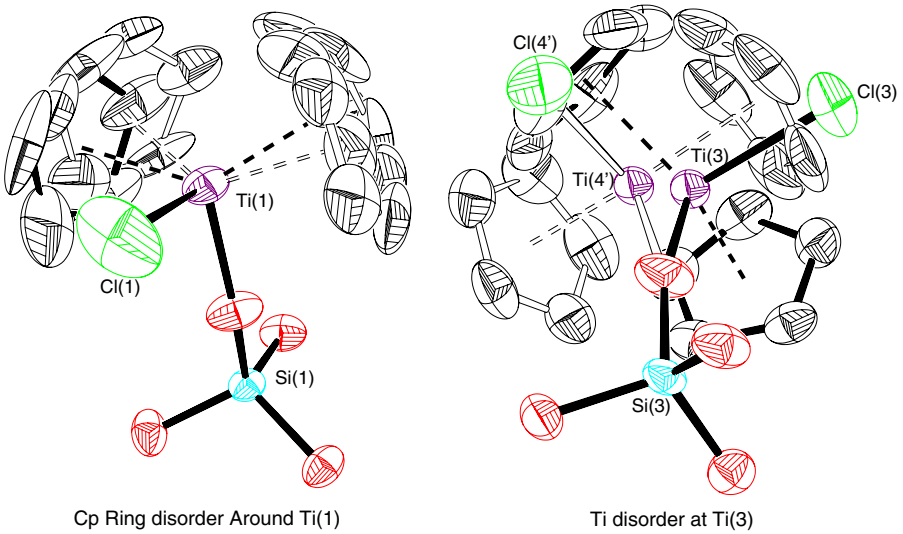

Fig. 5. The two types of disorder around the titanium atoms in the single crystal X-ray structure of $Si_8O_{20}(Cp_2TiCl)_8 \cdot 3CH_2Cl_2$.

Ti(3) and Ti(4) constitute one set of adjacent titanium atoms across an edge of the Si_8O_{20} core (Part 1) while Ti(4′) and Ti(3′) represent the second set of titanium positions (Part 2). The Cp_2TiCl groups are also disordered between two positions related by a 90° rotation around the Ti–O bond. The occupation of the two components was modeled by a standard floating occupancy free variable and was found to be approximately 1.5:1 for both titanocene groups (Ti(3)/TI(4′) and Ti(4)/Ti(3′)).

One methylene chloride solvate molecule is nondisordered but only occurs as one half of an equivalent per cube in the crystal. The other solvate molecule occurs as a full equivalent but is disordered roughly equally between two orientations that share the same central carbon position. The two orientations are related to one another by rotation of the Cl–C–Cl plane around the C_2 axis through the central carbon.

3.4. Structural characterization of $Si_{10}O_{25}(SnMe_3)_{10} \cdot 4H_2O$ (II)

$Si_{10}O_{25}(SnMe_3)_{10} \cdot 4H_2O$ crystallizes in the *Pcba* space group. Structural and refinement data are given in Table 1. The structure of the decakis trimethyl tin silicate (**II**) tetrahydrate in the crystal may be described as a highly distorted, pentagonal prism of five Si_4O_4 rings each sharing two edges (Fig. 6). The ten trimethyltin groups are bound to ten oxygen atoms external to the silicate cage. Four water molecules are also present in the crystal. Three of the four molecules are Lewis base adducts with tin and the fourth water is hydrogen bonded to an *exo*cage oxygen belonging to the silicate molecule. The two pentagonal faces making up the spherosilicate cage are not symmetrical due to "puckering" of corresponding Si–O–Si edges of the two opposite faces, similar to what is observed in other $Si_{10}O_{15}$ containing structures [2,51,59].

Three of the trimethyltin groups in $Si_{10}O_{25}(SnMe_3)_{10}$ are disordered. Two have tin atoms occupying two sites ((Sn10) and Sn(11)) with one of the methyl groups (C(25)) occupying the same position and the other four methyls (C(30) and C(32) bound to Sn(10) and C(29) and C(31) bound to Sn(11)) disordered between two positions (see Supplementary information). In the third trimethyltin group, the tin is disordered between two sites with occupancies of 95% and 5%. The positions of all three methyl group carbons associated with the more prevalent tin position have been located. Due to the low occupancy of the other tin site, none of the associated methyl groups could be located. No disorder in the $Si_{10}O_{15}$ cage was observed.

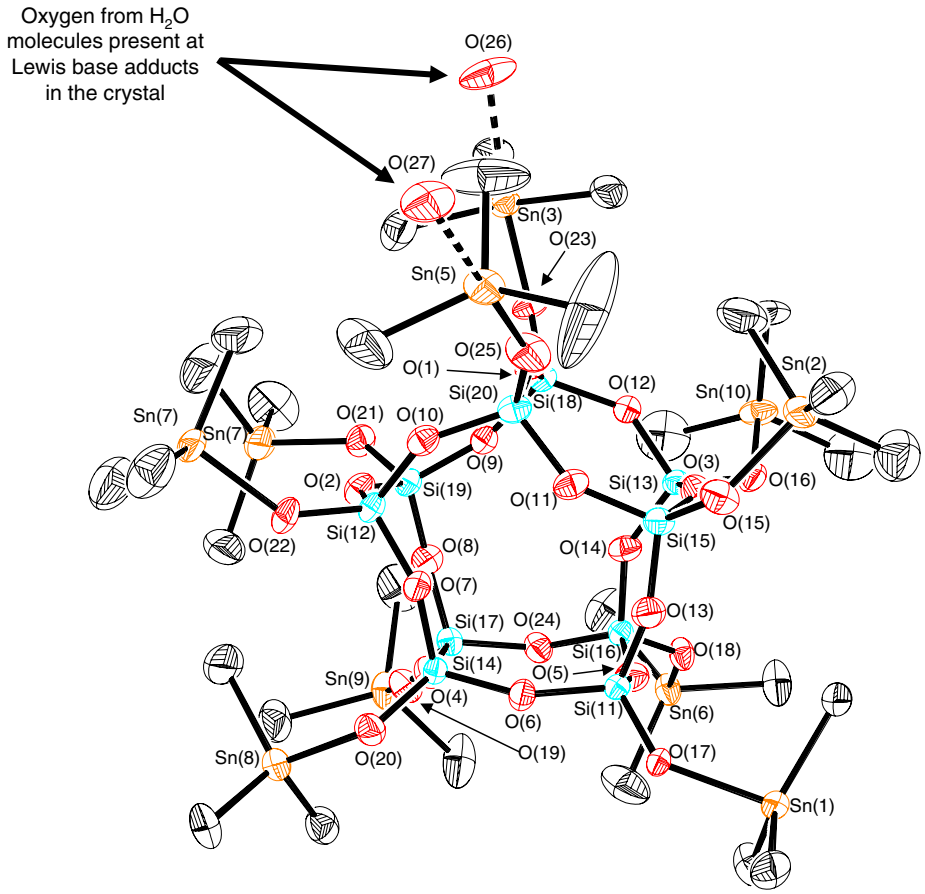

Fig. 6. Single crystal X-ray structure of $Si_{10}O_{25}(SnMe_3)_{10} \cdot 4H_2O$. The two oxygen atoms that have been assigned to water molecules which are present as Lewis base adducts with the tin atoms are shown.

The water molecules present in this structure are found as either Lewis base adducts, hydrogen bounded, or a combination of both as previously stated. The interactions observed for one water molecule are quite similar to that described in the tetrahydrate of $Si_8O_{12}(SnMe_3)_8$. For two of the water molecules, a similar type of interaction is observed where the oxygen from the water interacts with a tin group, but only one hydrogen of the water molecule interacts with a terminal oxygen bearing a trimethyltin group of a neighboring $Si_{10}O_{25}(SnMe_3)_{10}$ molecule. The last water does not show any specific interaction with tin. One of the hydrogen atoms of this water molecule appears to be hydrogen bonded to an oxygen bearing a trimethyltin group.

Much like in the **I · 4H$_2$O** structure, a consequence of the combination of Sn···O interactions and hydrogen bonding is the occurrence of two-dimensional planes of $Si_{10}O_{25}(SnMe_3)_{10}$ molecules in the solid state.

3.5. Structural comparisons of the Si_8O_{20} cage in **I**, **I · 4H$_2$O**, and **III** with other cubic silicates

Si_8O_{20} cage units have been described as rigid SiO_4 tetrahedra connected through Si–O–Si siloxy linkages [11]. The SiO_4 tetrahedra in **I**, **I · 4H$_2$O**, exhibit typical bond lengths and O–Si–O angles quite close to ideal values. However, the structures of **I** and **I · 4H$_2$O** are unusual in that the cubic Si_8O_{20} unit is considerably elongated along an axis perpendicular to a pair of opposite faces of the cube. This pair of Si_4O_4 faces is also compressed with respect to Si···Si separations along their Si–O–Si edges. The observed elongation and compression are due to opening and closing of the Si–O–Si angles parallel to the distortion axis and within the faces, respectively (Fig. 7). Two Si–O–Si angles approach linearity having observed angles of 172.1(1)° and 171.1(1)° while corresponding angles within the faces are quite small (136.3(1)° and 137.2(1)°) (Fig. 7). Previous studies of silicate cage structures presented analyses of average Si–O–Si and O–Si–O angles within zeolite and silicate minerals [11]. In the present study this approach would have masked the pronounced distortion seen in the tetrahydrate **I · 4H$_2$O** as the average of the minimum and maximum values given above (154°) is quite close to the average found in the CSD data. The individual angles observed in **I · 4H$_2$O** are among the largest and smallest reported for any structure containing the D4R fragment. The anhydrous trimethyl tin analogue **I**, also shows a similar type of distortion in the cage, but not nearly as pronounced.

The unusually large and small angles observed in the cage units of these two structures correlate with a splitting of the symmetric and antisymmetric Si–O–Si stretches observed in the IR for Si_8O_{20} cages. When compared to the titanocene analogue **III**, which has a more typical, symmetrical cage unit two resolvable signals corresponding to ν_{as}(Si–O–Si) and ν_s(Si–O–Si) vibrational modes were observed in **I** and **I · 4H$_2$O** (Fig. 8) [10,72]. The dependence of the Si–O–Si stretching frequencies has also been studied in glasses and it has been shown that the smaller this angle, the lower the value of the stretching frequency in the IR [72].

3.6. Structural comparisons of $Si_{10}O_{25}$ cage unit in $Si_{10}O_{25}(SnMe_3)_{10}$ with other pentagonal spherosilicates

The structure of the $Si_{10}O_{15}$ cage in **II** is unusual when compared to analogous decasilicate cage units. The SiO_4 tetrahedral subunits that make up this cage have a larger distribution of observed non-bonding O···O distances and O–Si–O angles around individual silicon atoms. This is evident in the plot of this angle as a function of the non-bonding O···O distance (see Supplementary information). In one case, a SiO_4 unit (Si(20)) in $Si_{10}O_{25}(SnMe_3)_{10}$ has an unusually small observed O–Si–O angle of 105.5(3)°. In fact all of the intracage O–Si–O angles associated with Si(20) are below that associated with a perfect

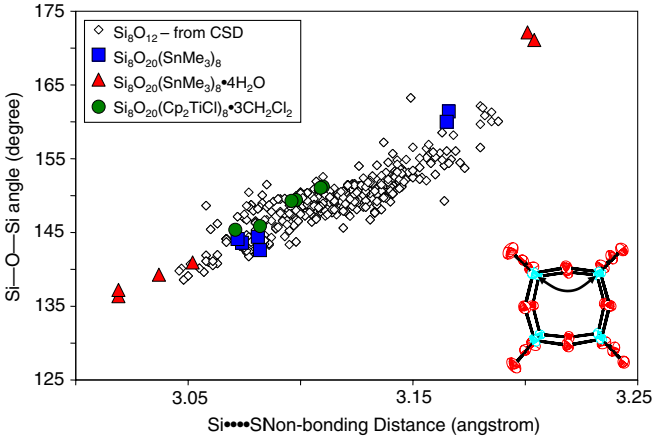

Fig. 7. Plot of Si–O–Si angles in Si_8O_{20} containing compounds discussed here as a function of non-bonding Si···Si distances. These data are superimposed on to that of other structures containing Si_8O_{12} cores reported in the CSD.

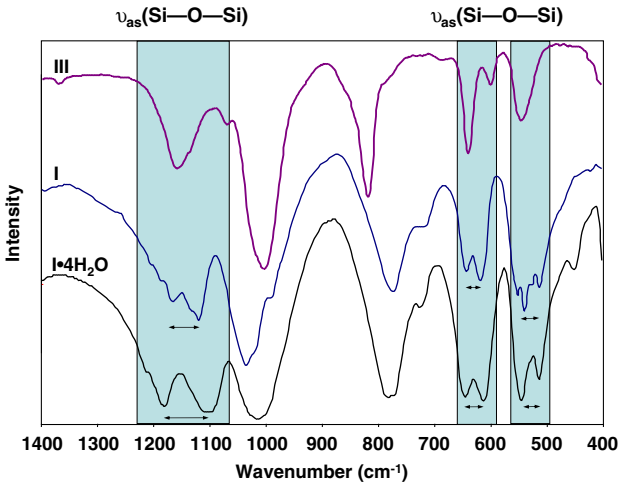

Fig. 8. IR spectra of **I**, **I · 4H$_2$O**, and **III** where the symmetric and asymmetric stretching Si–O–Si modes are highlighted.

SiO_4 tetrahedron (109.5°). As a consequence, the O–Si–O angles involving the *exo*cage oxygen are all quite large (110.2(3)°, 113.2(4)°, and 112.2(3)°). The trimethyltin group bound to this particular SiO_4 unit has a water molecule coordinated to the tin. However, another SiO_4 unit (Si(18)) in the molecule that also has a water molecule coordinated to tin does not exhibit the same type of distortion. We are not sure what the causes of distortions in the SiO_4 units at this time.

The observed Si–O–Si angles and non-bonding distances in $Si_{10}O_{25}(SnMe_3)_{10}$ also have a larger distribution of values than is observed in other structures containing $Si_{10}O_{15}$ units. This is observed in both the square and pentagonal faces. The Si–O–Si angles and distances found in the pentagonal faces of $Si_{10}O_{25}(SnMe_3)_{10}$ exhibit non-bonding Si···Si distances that are all slightly longer than what is observed in other D5R containing structures. The presence of the water molecules interacting both as Lewis bases with tin and hydrogen bonding to *exo*cage oxygen atoms may contribute to these structural features.

4. Conclusions

The synthesis and structures of several members of a family of trialkyltin derivatized spherosilicates have been described. The trialkyltin functionality allows for further reaction with metal chlorides as illustrated in the synthesis of $Si_8O_{20}(Cp_2TiCl)_8$. Comparisons with structural data for previous cubic and pentagonal prismatic containing spherosilicates indicate that SiO_4 tetrahedra in both Si_8O_{12} and $Si_{10}O_{15}$ spherosilicates are typically rather rigid and do not vary significantly from ideal values. Observed distortions in the cage units are mostly caused by variations in Si–O–Si angles connecting SiO_4 tetrahedra. The large distribution of the observed angles seen in the spherosilicates bearing trimethyltin groups may be due to the presence of Lewis base and hydrogen-bonding interactions between water in the crystal with tin groups of stannylated spherosilicates and *exo*cage oxygen atoms.

The structural variations observed for spherosilicate building units found in the compounds described herein are important because they are the basic building units present in many zeolites and silicates [11]. The molecular dimensions of these silicate cage units fall into the nanoscale size regime. Furthermore, they are both chemically and thermally robust. These properties make them attractive candidates as building blocks for the construction of mesoscopically designed solids [23]. Materials produced from such methods could have a wide applicability in the areas of catalysis and materials chemistry.

Acknowledgements

We gratefully acknowledge the support of the DOE (DE-FG02-00ER15259) and the Petroleum Research Fund (42634-AC5) for support of this research.

Appendix A. Supplementary information

Plot of O–Si–O angle vs. O···O separation for **II**. Crystallographic data (CIF files) for compounds **I** (CCDC 279729), **I · 4H$_2$O** (CCDC 279730), **II** (CCDC 279728) and **III** (CCDC 279731) have been deposited with the Cambridge Crystallographic Data Center and copies of this information is available free of charge at www.ccdc.cam.ac.uk/data_request/cif, or by e-mailing data_request@ccdc.cam.ac.uk, or by contacting The Cambridge Crystallographic Data Center, 12 Union Road, Cambridge CB2 1ES, UK; fax: +44 1223 336 033. Supplementary data associated with this article can be found, in the online version, at doi:10.1016/j.jorganchem.2006.03.028.

References

[1] P.G. Harrison, J. Organomet. Chem. 542 (1997) 141–183.
[2] N. Auner, B. Ziemer, B. Herrschaft, W. Ziche, P. John, J. Weis, Eur. J. Inorg. Chem. (1999) 1087–1094.
[3] M. Paech, R. Stoesser, J. Phys. Chem. A 101 (1997) 8360–8365.
[4] Y. Hayashino, T. Isobe, Y. Matsuda, Chem. Phys. Chem. 2 (2001) 748–750.
[5] B. Hong, T.P.S. Thoms, H.J. Murfee, M.J. Lebrun, Inorg. Chem. 36 (1997) 6146–6147.
[6] A. Provatas, M. Luft, J.C. Mu, A.H. White, J.G. Matisons, J. Organomet. Chem. 565 (1998) 159–164.
[7] M. Baertsch, P. Bornhauser, G. Calzaferri, R. Imhof, Vib. Spectrosc. 8 (1995) 305–308.
[8] H.B. Buergi, K.W. Toernroos, G. Calzaferri, H. Buergy, Inorg. Chem. 32 (1993) 4914–4919.
[9] Y. Huang, Z. Xu, E.A. Havenga, I.S. Butler, Vib. Spectrosc. 22 (2000) 175–180.
[10] C. Marcolli, P. Laine, R. Buehler, G. Calzaferri, J. Tomkinson, J. Phys. Chem. B 101 (1997) 1171–1179.
[11] A.M. Bieniok, H.-B. Buergi, J. Phys. Chem. 98 (1994) 10735–10741.
[12] D. Hoebbel, G. Garzo, G. Engelhardt, R. Ebert, E. Lippmaa, M. Alla, Z. Anorg. Allg. Chem. 465 (1980) 15–33.
[13] D. Hoebbel, W. Wieker, P. Franke, A. Otto, Z. Anorg. Allg. Chem. 418 (1975) 35–44.
[14] F.J. Feher, K.J. Weller, Inorg. Chem. 30 (1991) 880–882.
[15] V.W. Day, W.G. Klemperer, V.V. Mainz, D.M. Millar, J. Am. Chem. Soc. 107 (1985) 8262–8264.
[16] F.J. Feher, K.D. Wyndham, R.K. Baldwin, D. Soulivong, J.D. Lichtenhan, J.W. Ziller, Chem. Commun. (1999) 1289–1290.
[17] C.S. Brevett, P.C. Cagle, W.G. Klemperer, D.M. Millar, G.C. Ruben, J. Inorg. Organomet. Polym. 1 (1991) 335–342.
[18] T.J. Barton, L.M. Bull, W.G. Klemperer, D.A. Loy, B. McEnaney, M. Misono, P.A. Monson, G. Pez, G.W. Scherer, J.C. Vartuli, O.M. Yaghi, Chem. Mater. 11 (1999) 2633–2656.
[19] I. Hasegawa, K. Hibino, K. Takei, Appl. Organomet. Chem. 13 (1999) 549–554.
[20] C. Zhang, F. Babonneau, C. Bonhomme, R.M. Laine, C.L. Soles, H.A. Hristov, A.F. Yee, J. Am. Chem. Soc. 120 (1998) 8380–8391.
[21] C.L. Soles, E.K. Lin, W.-L. Wu, C. Zhang, R.M. Laine, Mater. Res. Soc. Sympos. Proc. 628 (2001) CC4.2.1–CC4.2.6.
[22] M.H. Lamm, T. Chen, S.C. Glotzer, Nano Lett. 3 (2003) 989–994.
[23] N.N. Ghosh, J.C. Clark, G.T. Eldridge, C.E. Barnes, Chem. Commun. (2004) 856–857.
[24] F.J. Feher, K.J. Weller, Chem. Mater. 6 (1994) 7–9.
[25] G.M. Sheldrick, A Program for the Refinement of Crystal Structures, University of Gottingen, Gottingen, Germany, 1997.
[26] G.M. Sheldrick, University of Gottingen, Gottingen, Germany, 1996.

[27] O. Kennard, F.H. Allen, M.D. Brice, T.W.A. Hummelink, W. D.S. Motherwell, J.R. Rodgers, D.G. Watson, Pure Appl. Chem. 49 (1977) 1807–1816.
[28] N.V. Podberezskaya, I.A. Baidina, V.I. Alekseev, S.V. Borisov, T.N. Martynova, Zh. Strukt. Khim. 22 (1981) 116–119.
[29] Y.I. Smolin, Y.F. Shepelev, R. Pomes, D. Hoebbel, W. Wieker, Kristallografiya 20 (1975) 917–924.
[30] Y.I. Smolin, Y.F. Shepelev, I.K. Butikova, Kristallografiya 17 (1972) 15–21.
[31] M.A. Said, H.W. Roesky, C. Rennekamp, M. Andruh, H.-G. Schmidt, M. Noltemeyer, Angew. Chem., Int. Ed. 38 (1999) 661–664.
[32] Y.F. Shepelev, Y.I. Smolin, A.S. Ershov, O. Rademacher, G. Sheller, Kristallografiya 32 (1987) 1399–1403.
[33] M. Wiebcke, D. Hoebbel, J. Chem. Soc., Dalton Trans. (1992) 2451–2455.
[34] M. Rattay, D. Fenske, P. Jutzi, Organometallics 17 (1998) 2930–2932.
[35] R. Tacke, A. Lopez-Mras, W.S. Sheldrick, A. Sebald, Z. Anorg. Allg. Chem. 619 (1993) 347–358.
[36] R. Duchateau, R.A. Van Santen, G.P.A. Yap, Organometallics 19 (2000) 809–816.
[37] G. Calzaferri, R. Imhof, K.W. Tornroos, J. Chem. Soc., Dalton Trans. (1994) 3123–3128.
[38] Y.I. Smolin, Y.F. Shepelev, R. Pomes, Khimiya Silikatov i Oksidov (1982) 68–85.
[39] N. Auner, J.W. Bats, D.E. Katsoulis, M. Suto, R.E. Tecklenburg, G.A. Zank, Chem. Mater. 12 (2000) 3402–3418.
[40] L. Ropartz, D.F. Foster, R.E. Morris, A.M.Z. Slawin, D.J. Cole-Hamilton, J. Chem. Soc., Dalton Trans. (2002) 1997–2008.
[41] K. Larsson, Arkiv foer Kemi 16 (1960) 203–208.
[42] G. Koellner, U. Mueller, Acta Crystallogr., Sect. C C45 (1989) 1106–1107.
[43] V.E. Shklover, Y.T. Struchkov, N.N. Makarova, K.A. Andrianov, Zh. Strukt. Khim. 19 (1978) 1107–1119.
[44] M.A. Hossain, M.B. Hursthouse, K.M.A. Malik, Acta Crystallogr., Sect. B B35 (1979) 2258–2260.
[45] G. Calzaferri, R. Imhof, K.W. Toernroos, J. Chem. Soc., Dalton Trans. (1993) 3741–3748.
[46] M. Wiebcke, J. Emmer, J. Felsche, D. Hoebbel, G. Engelhardt, Z. Anorg. Allg. Chem. 620 (1994) 757–765.
[47] J. Emmer, M. Wiebcke, J. Chem. Soc., Chem. Commun. (1994) 2079–2080.
[48] P.-A. Jaffres, R.E. Morris, J. Chem. Soc., Dalton Trans. (1998) 2767–2770.
[49] M. Nowotny, T. Maschmeyer, B.F.G. Johnson, P. Lahuerta, J.M. Thomas, J.E. Davies, Angew. Chem., Int. Ed. 40 (2001) 955–958.
[50] S. Lucke, K. Stoppek-Langner, B. Krebs, M. Lage, Z. Anorg. Allg. Chem. 623 (1997) 1243–1246.
[51] G. Calzaferri, C. Marcolli, R. Imhof, K.W. Toernroos, J. Chem. Soc., Dalton Trans. (1996) 3313–3322.
[52] R.K. Harris, D.Y. Naumov, A. Samadi-Maybodi, J. Chem. Soc., Dalton Trans. (1996) 3349–3355.
[53] F.J. Feher, D.A. Newman, J.F. Walzer, J. Am. Chem. Soc. 111 (1989) 1741–1748.
[54] M. Wiebcke, H. Koller, Acta Crystallogr., Sect. B B48 (1992) 449–458.
[55] M. Wiebcke, M. Grube, H. Koller, G. Engelhardt, J. Felsche, Microporous Mater. 2 (1993) 55–63.
[56] U. Dittmar, B.J. Hendan, U. Floerke, H.C. Marsmann, J. Organomet. Chem. 489 (1995) 185–194.
[57] R.K. Harris, J.A.K. Howard, A. Samadi-Maybodi, J.W. Yao, W. Smith, J. Solid State Chem. 120 (1995) 231–237.
[58] N.V. Podberezskaya, S.A. Magarill, I.A. Baidina, S.V. Borisov, L.E. Gorsh, A.N. Kanev, T.N. Martynova, Zh. Strukt. Khim. 23 (1982) 120–129.
[59] I.A. Baidina, N.V. Podberezskaya, S.V. Borisov, V.I. Alekseev, T.N. Martynova, A.N. Kanev, Zh. Strukt. Khim. 21 (1980) 125–129.
[60] P.A. Agaskar, Inorg. Chem. 30 (1991) 2707–2708.
[61] D.A. Armitage, R.N. Robinson, E.W. Abel, Inorg. Synth. 17 (1977) 181–183.
[62] R.K. Grasselli, Topics Catal. 21 (2002) 79–88.
[63] A. Blaschette, D. Schomburg, E. Wieland, Z. Anorg. Allg. Chem. 571 (1989) 75–81.
[64] E.-M. Poll, S. Samba, R.D. Fischer, F. Olbrich, N.A. Davies, P. Avalle, D.C. Apperley, R.K. Harris, J. Solid State Chem. 152 (2000) 286–301.
[65] H. Hanika-Heidl, Thesis, 2002.
[66] I. Lange, D. Henschel, A. Wirth, J. Krahl, A. Blaschette, P.G. Jones, J. Organomet. Chem. 503 (1995) 155–170.
[67] K.C. Molloy, K. Quill, D. Cunningham, P. McArdle, T. Higgins, J. Chem. Soc., Dalton Trans. (1989) 267–273.
[68] L. Jaeger, B. Freude, A. Krug, H. Hartung, J. Organomet. Chem. 476 (1994) 163–171.
[69] M. Parvez, S. Ali, M. Mazhar, M.H. Bhatti, M.N. Khokhar, Acta Crystallogr., Sect. C C55 (1999) 1280–1282.
[70] R. Eckhardt, H. Hanika-Heidl, R.D. Fischer, Chem. Eur. J. 9 (2003) 1795–1804.
[71] T.I. Ovsetsina, N.G. Furmanova, E.V. Chuprunova, V.I. Sheherbakov, Kristallografiya 38 (1993) 71–76.
[72] M. Tomozawa, J.W. Hong, S.R. Ryu, J. Non-Cryst. Solids 351 (2005) 1054–1060.